Meccanica
https://doi.org/10.1007/s11012-024-01850-x

RESEARCH

A computed tomography-based limit analysis approach to investigate the mechanical behavior of the human femur prone to fracture

Cristina Falcinelli · Aurora Angela Pisano · Marcello Vasta · Paolo Fuschi

Received: 4 December 2023 / Accepted: 3 July 2024

Abstract The paper proposes a refined CT-based FE modelling strategy that implements a limit analysis numerical procedure, namely the Elastic Compensation Method (ECM), to estimate a lower bound to the collapse load of a human femur. In particular, the model geometry was obtained from CT images by segmentation of a fresh-frozen human cadaveric femur that was discretized with second-order tetrahedral 3D finite elements. A yield criterion of Tsai–Wu-type, expressed in principal stress space, was adopted to model the bone tissues for which the strength limit values in tension, compression and shear are computed locally from the femoral density distribution also derived from CT images. The developed CT-based numerical technique showed the ability to predict, at least for the examined femur for which the experimental collapse load is available, a lower bound to the collapse load. The proposed approach seems a promising and effective tool that could be adopted into clinical practice to predict the fracture risk of human femur starting from patient-specific data given by medical imaging.

Keywords Femur mechanics · Limit analysis · Peak load prediction · CT-based FE modelling

C. Falcinelli (✉) · M. Vasta
Department of Engineering and Geology, University "G. D'Annunzio" of Chieti-Pescara, Viale Pindaro, 65127 Pescara, Italy
e-mail: cristina.falcinelli@unich.it

M. Vasta
e-mail: mvasta@unich.it

A. A. Pisano · P. Fuschi
Department of Heritage-Architecture-Urbanism, University Mediterranea of Reggio Calabria, Viale dell'Università, 89124 Reggio Calabria, Italy
e-mail: aurora.pisano@unirc.it

P. Fuschi
e-mail: paolo.fuschi@unirc.it

1 Introduction

Osteoporosis represents one of the major causes of femur fracture. An osteoporotic femur is characterized by low bone mass, microarchitectural deterioration and thus a significant loss of mechanical integrity [1, 2]. All these factors make the bone more prone to fracture. Currently, clinical practice determines fracture risk relying on areal bone mineral density (aBMD) measured by Dual-energy X-ray Absorptiometry [3]. The aBMD of a patient is related to a reference value for young adults of the same sex by using the T-score which is expressed in standard deviations (SDs). The T-score describes the number of SDs by which the aBMD in an individual differs from the mean value expected in young healthy individuals [4]. The diagnosis of osteoporosis is defined as a value for aBMD 2.5 SD or more below the young female adult mean (T-score less than or equal to −2.5 SD). However, aBMD and thus T-score are not always effective for identifying cases at high risk of fracture

Published online: 17 July 2024

[5]. The aBMD measured by DXA provides only a two-dimensional (2D) projection of a three-dimensional (3D) structure and cannot capture 3D bone geometry and micro-structure. Moreover, the DXA-based aBMD does not account for many mechanical phenomena affecting the bone strength that concur to femur fracture [6, 7]. As a result, the fracture risk assessment is a challenging task for clinicians. In this context, an impressive number of patient-specific finite element (FE) models of the femur from Computed Tomography (CT) images have been developed [8–11] to overcome aBMD limitations in identifying cases at high risk of fracture being able to better model the personalized mechanical determinants of fracture. While they are able to improve the prediction of ex-vivo measured femoral strength when compared to aBMD [12–14], in in-vivo applications the improvement over DXA-based aBMD in predicting, for example, hip fracture risk is different among the studies and depends mainly on the clinical patient cohort investigated [15–18].

The interest in this problem has stimulated different research strategies proposed in the relevant literature. However, some approaches, such as those implying the implementation of damage and fracture propagation models [9, 19, 20] or which investigate post-elastic phenomena up to failure [21, 22], although interesting from a research point of view, are currently not easily applicable to real problems especially in 3D modelling. In the Authors' opinion, mechanics-based approaches, not dependent on the identification of the elastic characteristics of the material as well as on accurate post-elastic modelling, but oriented to predict just the peak load of the bone at a state of incipient collapse may add a significant improvement in a reliable prediction of bone fracture risk.

In this context, Limit Analysis structural theory may represent an interesting approach towards the improvement of femoral fracture risk assessment. As well known, Limit Analysis allows to predict, with a high degree of accuracy, the collapse load of a structure by only knowing a field of admissible stresses normally defined by a stress-based constitutive criterion (Appendix 1). With respect to other strategies in the literature, the main advantage of the Limit Analysis is its ability to estimate the collapse load independently of the deformation or loading history without describing post-elastic phenomena, damage or fracture propagation. In the present work, the idea was to apply this theory in the context of bone biomechanics to assess its ability in predicting the collapse load for a human bone. To this aim, a Limit Analysis approach, whose robustness has already been experimented in different engineering contexts [23, 24], is herein adopted. A first attempt in the same direction can be found in Pisano et al. [25]. In that work, the theory of Limit Analysis was applied to investigate the proximal human femur in sigle-stance leg and sideways fall configurations under quasi-static loads. In particular, following the static theorem of Limit Analysis, a numerical procedure, that allows to evaluate a lower bound to the collapse load of the femur, has been implemented. The procedure involves a series of elastic analyses, each one carried on for acting loads greater than the ones used in the previous analysis, and is named Elastic Compensation Method (ECM). Indeed, during each analysis, the elastic moduli of the "femur materials" are appropriately varied/compensated to obtain a redistribution of the stresses that comply with an admissible stress domain, as stated by the static approach of limit analysis. The procedure is iterative and stops when, by increasing the loads, the redistribution of the stresses is no longer possible. However, in the above quoted paper, the ECM procedure was implemented considering a simplified 3D femoral geometry and, furthermore, unchanged values set for the strengths of the constituent materials (cortical, trabecular, marrow) along the whole the femur. In a more recent work [26] a sensitivity analysis has been performed by evaluating the influence of the cortical and trabecular thicknesses and strengths on the numerical findings. The great sensitivity shown by the results, in terms of the predicted ultimate load, demonstrates the need for a more accurate modeling of both the geometry and the strength quantities.

To overcome the weaknesses present in Pisano et al. [25, 26] this paper proposes a CT-based Limit Analysis numerical approach. The novelties of the present approach can be summarized as follows: first, a realistic femoral geometry reconstructed from CT images has been obtained; second, all the constitutive parameters have been derived locally, i.e. point by point, as a function of the femoral density distribution that has been obtained from the CT images; finally, a quantitative validation, considering a comparison with real/experimental data

on a specific real femur, has been performed. It is important to underline that the proposed method is of general applicability, since it allows to take into account the loss of resistance correlated to reduction, if any, of bone density in specific areas. The procedure is not specifically oriented to diseased femurs but it can easily take into account the presence of tumors, osteophytes or other pathologies that influence the strength values of the bone tissues which, as will be clarified below, are the driving material parameters of the analysis.

The paper is organized as follows. In Sect. 2 both the computational modelling procedure with the constitutive assumptions and the numerical implementation are described. The main results are reported in Sect. 3. Discussion and concluding remarks are reported in Sects. 4 and 5, respectively. Finally Appendix 1 reports some very basic concepts of Limit Analysis theory, whereas in Appendix 2 a flow diagram of the numerical implementation is showed.

2 Material and methods

The left fresh-frozen cadaveric femur of a female, 76 years old, 160 cm in height, 50 kg, who died of renal cell cancer has been selected among the specimens used in [27]. The femur was characterized by a metastasis located in the femoral neck and was experimentally tested under single leg stance loading configuration up to fracture which was registered at an ultimate load of 4500 N [27]. The choice to investigate a metastatic femur was merely due to the full availability of experimental findings for this case; as said above the procedure is not only applicable in case of tumor diseases.

2.1 Computational modelling procedure

2.1.1 CT imaging

As described in [27], the femur was CT-scanned (Phillips Brilliance 64 CT axial scanner, Eindhoven, Netherlands) with a K_2HPO_4 calibration phantom. The following CT scanner parameters have been used for the acquisition: 120 kVp, 250 mAs, 1.25 mm slice thickness, and $0.2 \cdot 0.2$ mm pixel size.

2.1.2 Geometry reconstruction and FE meshing

First, the CT images were segmented using a semi-automatic procedure to reconstruct the femoral geometry considering the portion of the femur comprised from the mid-diaphysis to the femoral head (ITK-Snap 3.2.0, University of Pennsylvania) (Fig. 1). The cartesian reference system is characterized by the z axis aligned with the diaphyseal axis, the x axis oriented in the medio-lateral direction or radial direction and the y axis aligned in antero-posterior direction. Then, femur geometry has been meshed through second-order displacement-based tetrahedral elements in Comsol Multiphysics (Comsol, v.6.0 COMSOL, Stockholm, Sweden). The FE-mesh was characterized by $6.2 \cdot 10^5$ elements with an average element side size of about 1.5 mm (Fig. 1).

As will appear clearer below, such a dense discretization is important because it allows us to consider, within each element of the FE model, the actual tissue strength parameters, evaluated through CT images. Moreover, a finer mesh allows to implicitly account for the presence of osteoporosis, tumors or other pathologies that influence the values of these parameters and, consequently, the evaluation of the collapse load of the femur. Finally, a dense discretization is used to better capture the thin cortical thickness that characterizes the proximal femur with the aim of reducing the partial volume effect (PVE) that impacts the finite element results. Regarding the convergence behavior of the numerical model it is important to highlight that the ECM, grounding on elastic analyses, does not have particular numerical drawbacks of convergence related to the mesh configuration. The element size of the mesh exhibits the usual limitations of all the displacement based FE procedures that determine the stress as secondary variables.

2.1.3 Material's model and constitutive assumptions

Cortical and trabecular bone tissues have been assumed to be characterized by a transversally isotropic and orthotropic behavior, respectively. The corresponding constitutive parameters have been obtained from the density distribution derived from the CT images. In detail, the density distribution has been obtained by interpolating the Hounsfield Unit (*HU*) value of each CT voxel and then applying empirical relationships. Specifically:

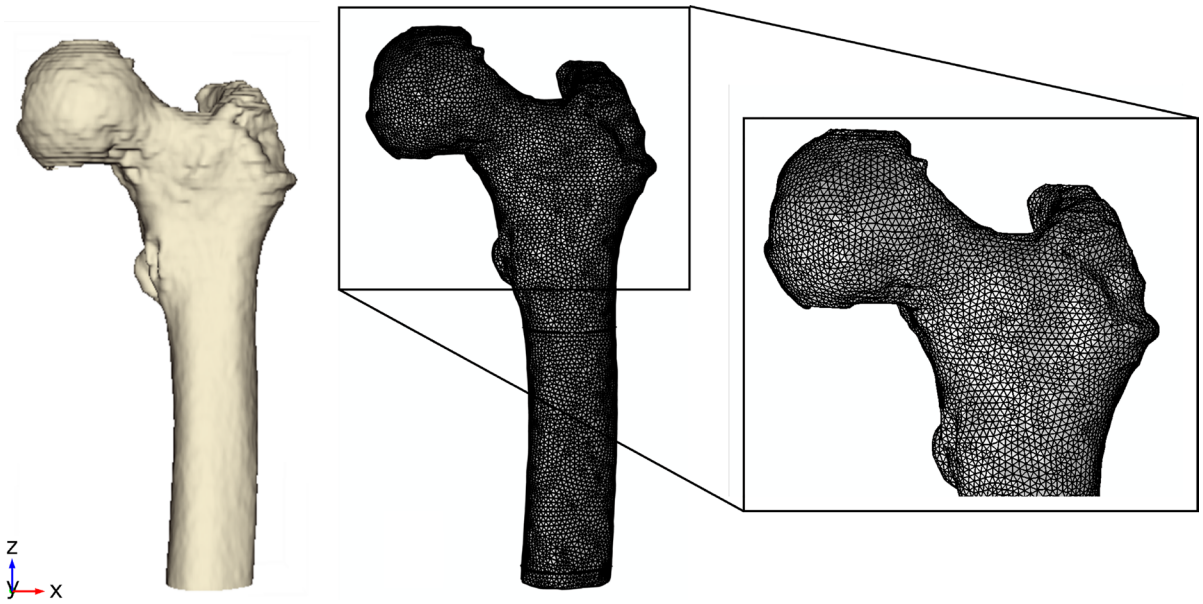

Fig. 1 Femur geometry reconstructed by segmenting the CT dataset (left) and second-order displacement-based tetrahedral mesh (right)

- HU values were converted to equivalent mineral density values ($\rho_{K_2PO_4}$, g/cm^3) through the following calibration equation that was obtained using a K_2PO_4 liquid phantom [27]:

$$\rho_{K_2PO_4} = 10^{-3} \times (0.8072 \times HU - 1.6); \quad (1)$$

- ash density (ρ_{ash}, g/cm^3) was calculated using $\rho_{K_2PO_4}$ density through the following relation [27]:

$$\rho_{ash} = 0.877 \times 1.21 \times \rho_{K_2PO_4} + 0.08; \quad (2)$$

- apparent density (ρ_{app}, g/cm^3) was derived from the ρ_{ash} ($\rho_{ash}/\rho_{app} = 0.6$) [28]. Figure 2 shows the distribution of ρ_{app} along the femur. To address the PVE in the region where the cortex is thin as the femoral neck, the ρ_{app} at any node of the bone surface has been compared to the corresponding value of the nearest internal node. If the value of ρ_{app} was lower than the ρ_{app} of the nearest internal node, the apparent density of the node of bone surface has been corrected and the ρ_{app} of the nearest internal node has been assigned to this node.

To derive the elastic material properties the relationships used in [29] have been implemented. In detail the following relationships have been used:

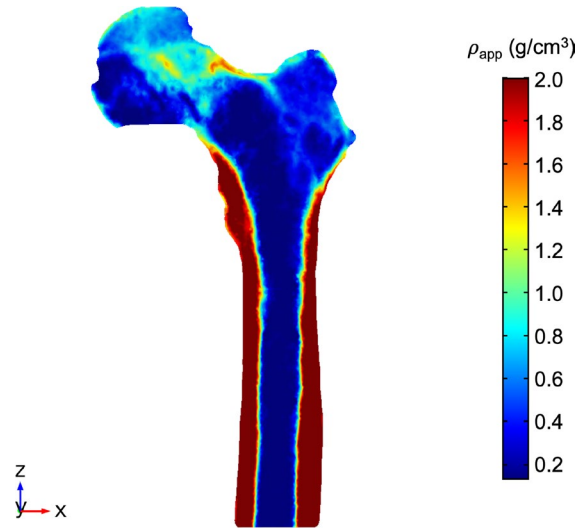

Fig. 2 Distribution of ρ_{app} in a coronal section of femur ($y = 205$ mm)

- for trabecular bone ($\rho_{app} < 0.81$ g/cm^3)

$$E_{33} = 2671\rho_{app}^{2.29};$$
$$E_{11}/E_{33} = 0.47\rho_{app}^{0.12} \quad (3)$$
$$E_{22}/E_{33} = 0.76\rho_{app}^{0.09}$$

$$G_{12}/E_{33} = 0.26\rho_{app}^{0.24}$$
$$G_{32}/E_{33} = 0.29\rho_{app}^{0.17} \quad (4)$$
$$G_{13}/E_{33} = 0.45\rho_{app}^{0.18}$$

$$\nu_{12} = 0.27\rho_{app}^{-0.09}$$
$$\nu_{13} = 0.14\rho_{app}^{-0.16} \quad (5)$$
$$\nu_{23} = 0.14\rho_{app}^{-0.07}$$

- for cortical bone ($\rho_{app} \geq 0.81\,\mathrm{g/cm^3}$)

$$E_{33} = 2671\rho_{app}^{2.29}$$
$$E_{11}/E_{33} = 0.57 \quad (6)$$
$$E_{22}/E_{33} = 0.57$$

$$G_{12}/E_{33} = 0.2$$
$$G_{13}/E_{33} = 0.29 \quad (7)$$
$$G_{23}/E_{33} = 0.29$$

$$\nu_{12} = 0.4$$
$$\nu_{13} = 0.37 \quad (8)$$
$$\nu_{23} = 0.37$$

The material orthotropy has been accounted for by assuming the axes of the material reference system oriented in the following way: axis 1 oriented along the medio-lateral or radial direction; axis 2 aligned along the anterior-posterior direction; axis 3 oriented along the axis of diaphysis. As such, in the previous relationships, if the material parameter is labeled with 1 means that the material direction is mediolateral, if the parameter is labeled with 2 means that the material direction is anterior-posterior and if it is labeled with 3 the direction is axial.

It is important to underline that the real values of the elastic moduli, and of the related elasticity laws, are irrelevant for the determination of both the value of the collapse load here searched, as well as the type of collapse mechanism. This irrelevance, in the addressed context of plastic collapse analysis, can be explained by the concept of limit/collapse load itself. Indeed, the collapse mechanism initiates when the acting load reaches its limit value, leading to a deformation process of exclusively plastic nature that overlaps the state of stress as well as the elastic and plastic strains already accumulated at the moment of the incipient collapse. These, let's say, pre-collapse-stresses and pre-collapse-strains remain unchanged after the beginning of the collapse mechanism, the structure essentially behaving as if it were rigid in that state, but capable of producing incipient plastic strains. Due to the infinitesimal assumption of the mentioned pre-collapse-strains, by applying the principle of effects superposition, it can be assert that the mechanism of collapse can be studied neglecting the state of pre-collapse-strains and therefore considering the structure as if it were rigid-plastic. The rigid plastic model, often invoked by the plastic collapse design, underscores the idea that elastic strains, regardless of the specific constitutive law governing the material's behavior, are essentially irrelevant when determining collapse load and the associated collapse mechanism. For the reasons above, the Limit Analysis performed by ECM does not need the real elastic constants, however, to initialize the iterative ECM procedure one choice can be to start with a model that has the elastic moduli given by Eqs. (3–8).

For the evaluation of the collapse load is instead crucial the correct definition of bone strengths parameters which, in this article, unlike what was proposed in [25], have been derived from the bone density distribution of the femur. The strength limits were given by empiric correlations [30] according to experimental data reported in [31]. In particular, assuming that the indices $i = 1, 2, 3$ and $j = 1, 2, 3$ refer to the direction and plane of orthotropy, within the n^{th} finite element of the discretized model, the limit values in compression, tension, and shear are assumed in function of the ρ_{app} distribution and are given by the following relationships [30–32]:

$$\hat{\sigma}^{-}_{3,n} = 102\rho_{app,n}^{1.86} \quad (9)$$

$$\hat{\sigma}^{-}_{1,n} = \hat{\sigma}^{-}_{2,n} = 0.6\hat{\sigma}^{-}_{3,n} \quad (10)$$

$$\hat{\sigma}^{+}_{i,n} = \frac{1}{2}\hat{\sigma}^{-}_{i,n} \quad (11)$$

$$\hat{\sigma}_{ij,n} = 0.25\hat{\sigma}^{-}_{i,n} \tag{12}$$

It is worth to remark that the strengths parameters determine the admissible stress domain of the bone tissue and eventually the value of the collapse load.

2.1.4 Tsai–Wu yield criterion

For the femur's tissues a constitutive behavior that satisfies the Tsai–Wu criterion [33] was assumed. Precisely, the Tsai–Wu criterion is used to fix a stress admissible domain, herein named Tsai–Wu-type yield surface. Considering again the *n th* element of the FE mesh, the Tsai–Wu-type yield surface, in the principal stress space, can be written as [25]

$$\begin{aligned} G_{11,n}\sigma_{11,n}+G_{22,n}\sigma_{22,n} + G_{33,n}\sigma_{33,n} + F_{1111,n}\sigma^2_{11,n} \\ + F_{2222,n}\sigma^2_{22,n} + F_{3333,n}\sigma^2_{33,n}+ \\ 2F_{1122,n}\sigma_{11,n}\sigma_{22,n} + 2F_{1133,n}\sigma_{11,n}\sigma_{33} \\ + 2F_{2233,n}\sigma_{22,n}\sigma_{33,n} = 1 \end{aligned} \tag{13}$$

where $G_{ii,n}$, $F_{iiii,n}$ and $F_{iijj,n}$ are stress coefficients as specified below, while $\sigma_{11,n}$, $\sigma_{22,n}$ and $\sigma_{33,n}$ are the principal stresses. For the *n th* element, the stress coefficients are expressed by the following relationships:

$$G_{ii,n} = \frac{1}{\hat{\sigma}^{+}_{i,n}} - \frac{1}{\hat{\sigma}^{-}_{i,n}} \tag{14}$$

$$F_{iiii,n} = \frac{1}{\hat{\sigma}^{+}_{i,n}\hat{\sigma}^{-}_{i,n}} \tag{15}$$

$$F_{iijj,n} = \frac{1}{2}\left(\frac{1}{\hat{\sigma}^{+}_{i,n}\hat{\sigma}^{-}_{i,n}} + \frac{1}{\hat{\sigma}^{+}_{j,n}\hat{\sigma}^{-}_{j,n}} - \frac{1}{\hat{\sigma}^{2}_{ij,n}}\right) \tag{16}$$

in which $\hat{\sigma}^{+}_{i,n}$, $\hat{\sigma}^{-}_{i,n}$ and $\hat{\sigma}_{ij,n}$ are the strength limit values in tension, compression, and shear, respectively, as given by (Eqs. 9–12).

To ensure that the yield surfaces correspond to an ellipsoidal shape the following inequality must be also satisfied for each element:

$$F_{iiii,n}F_{jjjj,n} - F^2_{iijj,n} \geq 0. \tag{17}$$

It is important to highlight that each mesh element is characterized by a specific yield surface due to the fact that the strength limit values are density-dependent, see again Eqs. (9–12).

2.1.5 Loading and constraints

The femur is subjected to the load F_{ref} defined in the form of $F_{ref} = P_D p_{ref}$ with P_D a scalar design load multiplier (as will be better specified in Sect. 2.1.4) and p_{ref} a resultant reference load. In detail, p_{ref} has been defined as $p_{ref} = \sum_i p^i$ with p^i denoting the loads applied at all *i*-nodes located on a circular surface of 10 mm in diameter at the top of the femoral head with an orientation of 15°with respect to the diaphyseal axis (*z*-axis). Here, it has been considered that $p_{ref} = \sum_i p^i$ is equal to 1000 N. In terms of constraints, the distal part of the femoral shaft was fully fixed. The applied boundary and loading conditions reproduce indeed the experimental setup given in [27] to which the reader can refer for details.

2.2 Numerical implementation of limit analysis

The Limit Analysis (Appendix 1) has been implemented, in the shape of the above quoted ECM, within the commercial FE program Comsol Multiphysics (Comsol, v.6.0 COMSOL, Stockholm, Sweden).

The ECM is a FE-based iterative procedure aimed at calculating a lower bound multiplier P_{LB} of the collapse load that allows the construction of a femoral stress field that is statically and plastically admissible i.e. a field in which all the stress points are located inside or, at least, on the yield surface, being also satisfied the equilibrium conditions. The ECM performs a sequence of linear elastic analyses, each characterized by a fixed load multiplier P_D. For each sequence a certain number of iterations is carried out. Lets indicate with $v = 1...V$ the sequences of linear elastic analyses and with $k = 1...K$ the iterations in each sequence v. So, the first sequence of linear elastic analyses corresponds to $v = 1$. For a certain sequence v, the implementation starts to assign the load $F^v = P^v_D p_{ref}$ on the constrained femur. The multiplier P^v_D remains fixed during the sequence v. The term P^1_D represents the first starting value of the scalar design load multiplier. Under these conditions the first iteration k, i.e. the first linear elastic analysis of the sequence v, starts. During this iteration for each element n of the FE mesh the material moduli $E^{k-1}_{ij,n}$, $G^{k-1}_{ij,n}$

and $\nu_{ij,n}^{k-1}$ are assigned to the femur. In particular, for $k = 1$ the values of $E_{ij,n}^{k-1}$, $G_{ij,n}^{k-1}$ and $\nu_{ij,n}^{k-1}$ are expressed by Eqs. (3–8). At this point the first linear elastic analysis of sequence v is performed to calculate the associated stress field. In detail, for each element of the mesh a stress value is computed by averaging the principal stresses values computed within the Gauss Points of the element. For each element n this stress value corresponds to a point $\mathbb{P}_n^{k-1}$ in the principal stress space. Lets indicate with $\mathbb{O}$ the origin of this space. The quantity $\overrightarrow{\mathbb{OP}}_n^{k-1}/|\overrightarrow{\mathbb{OP}}_n^{k-1}|$ represents the direction that identifies the stress point $\mathbb{P}_n^{k-1}$ of the current element n in the principal stress space. In the same space the Tsai–Wu-type surface, pertinent to the specific element, is also represented. For the current element n lets then indicate with $\mathbb{P}_n^{Y(k-1)}$ the stress point lying on the corresponding Tsai–Wu surface on the direction $\overrightarrow{\mathbb{OP}}_n^{k-1}/|\overrightarrow{\mathbb{OP}}_n^{k-1}|$. If for the element n the quantity $|\overrightarrow{\mathbb{OP}}_n^{k-1}|$ results greater than $|\overrightarrow{\mathbb{OP}}_n^{Y(k-1)}|$ the stress point of the element is outside from the corresponding Tsai–Wu surface. For all elements for which this condition is verified (i.e. the pertinent Tsai–Wu yield condition is violated by the "element stress") the material element properties $E_{ij,n}^{k-1}$ and $G_{ij,n}^{k-1}$ are reduced using the following relationships

$$E_{ij,n}^{k} = E_{ij,n}^{k-1}\left[\frac{|\overrightarrow{\mathbb{OP}}_n^{Y(k-1)}|}{|\overrightarrow{\mathbb{OP}}_n^{k-1}|}\right]^2 \tag{18}$$

$$G_{ij,n}^{k} = G_{ij,n}^{k-1}\left[\frac{|\overrightarrow{\mathbb{OP}}_n^{Y(k-1)}|}{|\overrightarrow{\mathbb{OP}}_n^{k-1}|}\right]^2 \tag{19}$$

whereas, indeed, the Poisson ratios $\nu_{ij,n}^{k-1}$ are kept constant and thus $\nu_{ij,n}^{k} = \nu_{ij,n}^{k-1}$. Once the update of (element) material properties is completed (i.e. performed in all the elements whose stress $\mathbb{P}_n^{k-1}$ was outside the pertinent Tsai–Wu surface), the algorithm locate the maximum stress in the whole mesh, i.e. the stress point farthest away from Tsai–Wu-type surface, say $\mathbb{P}_{max}^{k-1}$, and locate the corresponding stress at yield, say $\mathbb{P}_{max}^{Y(k-1)}$. If $|\overrightarrow{\mathbb{OP}}_{max}^{k-1}|$ is greater than $|\overrightarrow{\mathbb{OP}}_{max}^{Y(k-1)}|$ the algorithm performs a new FE analysis, within the current elastic sequence v, under the same load $F^v = P_D^v p_{ref}$, but with the new (i.e. reduced where necessary) material parameters, calculated by Eqs. (18 and 19), to try to redistribute all the stresses out of the admissible domains. The iterations are performed until all stress points are below or reach their corresponding yield values. If this happens at the iteration $k = K$, at this iteration a statically and plastically admissible stress field is obtained and P_D^v is definitively a lower bound of the collapse load. Thus, a new sequence $v = v + 1$ of elastic analyses starts by setting the load as $F^{v+1} = P_D^{v+1} p_{ref}$ with $P_D^{v+1} > P_D^v$. The iterative stress redistribution procedure continues up to a further load increase does not allow all the stress points to be brought below or onto the yield surface. The greater value of P_D adopted in the iterative procedure for which the stresses can be redistributed gives the searched (maximum) lower bound multiplier P_{LB} and eventually, a (lower bound) prediction of the limit load $P_{LB} p_{ref}$.

It is worth noting that the iterative elastic analyses involved within the ECM are aimed to redistribute the stresses making the method very different either from an evolutive step-by-step analysis (grounded on elastic-predictor/plastic-corrector schemes) or from the so-called "element kill strategies". In the ECM, as effect of the redistribution, during the iterations the elements can change their stress state, from an elastic stress state to a stress state exceeding the yield value and viceversa.

Numerical simulations have been run on a multiprocessor Intel(R) Xeon(R) 8-core Bronze 3206R 16 GB of RAM, requiring averagely 1 h of computational time per each iteration k in each sequence v of FE analyses. In Fig. 5 a flow diagram of the ECM is shown.

3 Results

For the examined femur, a first sequence of elastic analyses started considering $P_D^1 = 3.0$. The value 4.2 is the maximum load multiplier for which it was possible to redistribute the stresses within all the FEs in the mesh. Therefore the computed P_{LB} is equal to 4.2 and the corresponding estimated failure load F_{LB} is 4200 N. This result is very encouraging as it represents an effective lower bound to the experimental collapse load recorded in 4500 N. In Fig. 3 the load multiplier versus iteration number is shown during the last redistributable sequence of FE analyses.

Figure 4 shows the distribution of the Von Mises stresses at the coronal section for the last converged sequence of the analysis. The values of these stresses

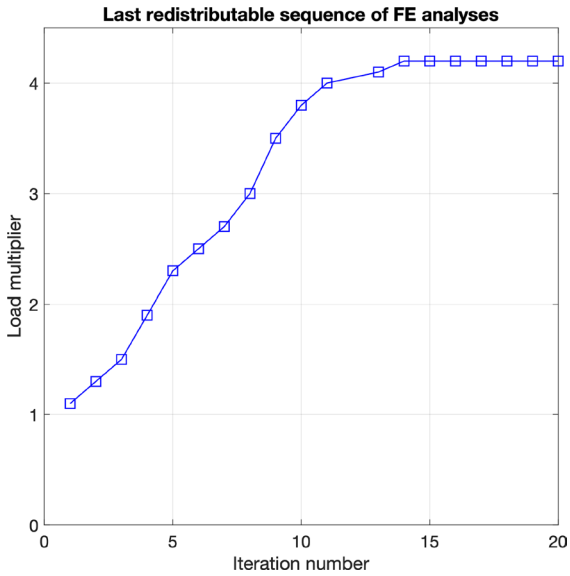

Fig. 3 The load multiplier versus iteration number during the last redistributable sequence of FE analyses

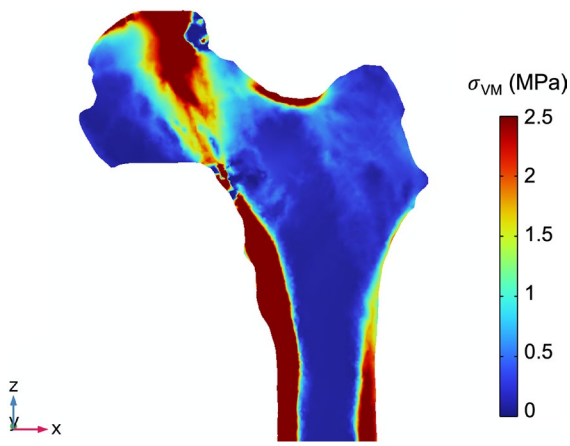

Fig. 4 Distribution of the von Mises stress measure (in MPa) at the coronal section $y = 205$ mm

are the real ones only in the portions of the bone exhibiting collapse where, as stated by Limit Analysis theory, the unicity of the stresses is assured. The stresses out of the zones where the collapse mechanism is at an incipient state are not unique and so they have only a qualitative nature. Nevertheless, the distribution of the Von Mises stresses at their threshold value shown in Fig. 4 locate the femur's zones in which failure/plastic mechanisms are at an incipient stage. It is worth noting how the areas of higher stresses are consistent with the failure mechanism recorded during the experimental test shown in Figure 8 in the paper [27].

4 Discussion

For the first time a CT-based FE modelling strategy has been applied within a numerical Limit Analysis method of general applicability, such as the ECM, to predict the collapse load of a real femur, for which are available experimental results. An accurate reconstruction of the femoral geometry, used for the elastic numerical analyses involved by the approach, has been obtained using CT images. Moreover, CT images have been used to derive a more coherent identification of the mechanical material parameters. The numerical method is robust and has the undoubted advantage of being based only on elastic analyses of the femur model and on the knowledge of bone's strength values. The small gap between the two failure load values, numerical and experimental, is particularly significant in this case of bone with tumor pathology for which it would not have been possible to take into account the reductions in strengths of some parts of the bone if not by assuming variable strengths values related to the density evaluated starting from CT images.

Even if the numerical result, in terms of predicted collapse load, is very good when compared with the experimental one, some limitations must be mentioned. The use of a single cadaveric femur represents one of the main limitations of the present work. The aim of this work was indeed to try to apply a well-established methodology in solid mechanics to a realistic femur deriving all parameters from CT images to understand the applicability and performance of the method. The application of such a method to bone was reported in [25]. In that work Pisano et al. [25] reported a good performance of the approach when

they compared their results with those available in the literature. However, they used a simplified geometry that can not account for subject-specific aspects of both bone geometry and material properties that may affect the mechanical response of the femur and thus the collapse load prediction. These subject-specific aspects can be included using CT images. In addition, deriving the information from diagnostic data as CT images open towards the application of the method in the clinical practice for the femur fracture risk assessment. Starting from this work and prior the application of this approach to clinical patients, the study needs to be extended to a wider sample size, as well as different loading conditions need to be investigated, to support and validate proposed preliminary findings and quantify the improvement with respect to other strategies developed in the literature. All these aspects will be object of future work. It is important to highlight that due to the limitation related to the use of a single femur, this first work must be considered as a proof-of-concept and the findings derived from this work can not be considered exhaustive and needed further investigations.

In the view to translate this approach into clinical practice it is important to account for multiple loading conditions spanning a domain of plausible force directions to identify subject-specific bone weakness as demonstrated in [15]. It is important to highlight that the proposed methodology is suitable to simulate static loading conditions but is limited in the view of application of dynamic loads.

Another limitation is represented by the empirical expressions used to move from bone density measurements to material strengths parameters. Furthermore, the metastasis present on the analyzed femoral neck was not treated with the aid of a different constitutive model, but was accounted for implicitly through the correlated reduction of bone density, and the consequent loss of resistance, of the involved area. As such, the possibility of incorporating a specific constitutive description for the metastatic region will be investigated in a future work.

Besides the model validation, the model verification, i.e. robustness and sensitivity analyses, is an important step to extract clinically relevant recommendations. Robustness of ECM approach has been proved by applying the method to structures made of different materials like composites, complying with a Tsai–Wu-type criterion [23, 34, 35], or reinforced concrete, obeying to a Menetrey-Willam-type criterion [24, 36, 37]. In terms of sensitivity analysis, a first investigation has been performed to evaluate the influence of the cortical and trabecular thicknesses and strengths values on the numerical prediction of femoral collapse load in a simplified geometry [26]. However, due to the importance of evaluating the influence of modelling choices on the estimation of collapse load, a deeper investigation about the influence of the relations used to derive the strength limit values from the CT-based bone density distribution using a realistic femur is of outmost importance.

Another validation of the use of Limit Analysis in this context would be the implementation of a numerical method based on the kinematic theorem of Limit Analysis, to be able to calculate an upper bound to the collapse load and therefore be aware of the actual range of values in which the true collapse load falls. The calculation of a lower bound may, in fact, be overly conservative.

Moreover, a consistent and precise identification/prediction of the collapse mechanism can be obtained by kinematic approach where the areas that are at an incipient collapse state are precisely located in terms of displacement rates distributions characterizing the real collapse mechanism. The application of a kinematic numerical method of Limit Analysis is the subject of an ongoing research work.

5 Conclusion

The article has presented the application of an iterative numerical procedure of Limit Analysis which uses only elastic analyses and needs only an accurate evaluation of the material strengths no matter of the real values of the elastic material constants. The procedure, known as Elastic Compensation Method, gives a prediction of the collapse load of a human femur. The numerical model was set up on the basis

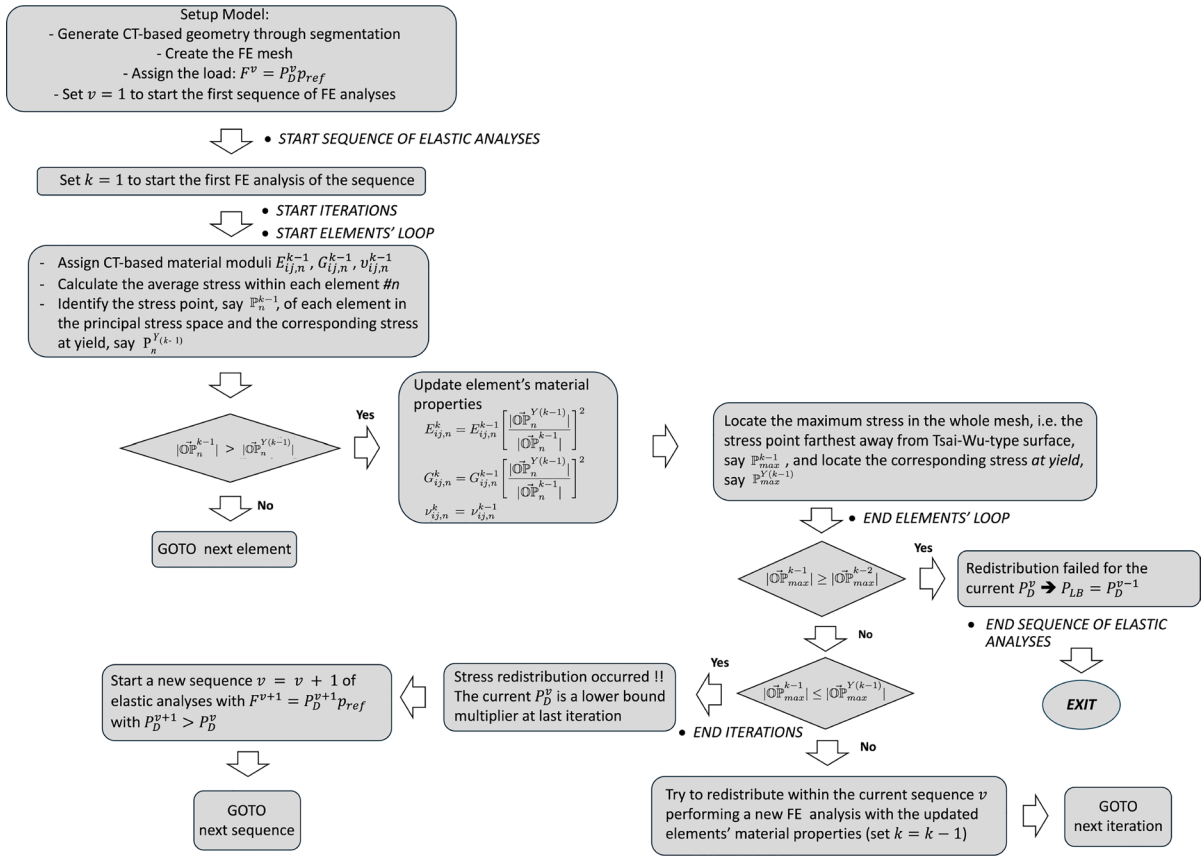

Fig. 5 Flow diagram of the elastic compensation method

of CT images obtained by segmentation of a cadaveric femur for which experimental data was available. The accurate CT based reconstruction of the femur geometry and the detailed evaluation of the density-based resistance parameters of the material has allowed the appropriate calibration of the numerical mechanical model giving a numerical prediction of collapse load very close to the one evaluated experimentally.

Even if a more robust validation of the method by expanding the sample size and the loading conditions is a mandatory step forward to validate proposed preliminary findings, the encouraging result may open towards to the possibility to apply the method to specific patients for their fracture risk assessment.

Acknowledgements Cristina Falcinelli and Marcello Vasta acknowledge the support of the Italian National Group for Mathematical Physics (GNFM-INdAM) and wish to thank the Italian Ministry of University and Research, through the PRIN PNRR 2022 funding scheme (Project title "MEchanics vs Cell competition: Hyperelasticity and Adaptation in Vascular Evolutionary Repair and Smart Endoprostheses" MECHAVERSE - Project code P2022M3KKC). Cristina Falcinelli acknowledges the funding by the European Union - Fondo Sociale Europeo - PON Ricerca e Innovazione 2014–2020 (azione IV.6) - FSE-REACT EU. Aurora Angela Pisano and Paolo Fuschi acknowledge the financial support by the Italian Ministry of University and Research (MUR), Progetti di Ricerca di Rilevante Interesse Nazionale, (PRIN) 2022 - Grant N. 20228CPHN5. The authors acknowledge Prof. Zohar Yosibash for providing the CT-scan images and the experimental data of the femur analyzed in this work.

Author contributions C.F.: Conceptualization, Methodology, Software, Data curation, Writing—original draft, Visualization, Investigation, Writing—review & editing. A.A.P.: Conceptualization, Methodology, Writing—review & editing. M.V.: Conceptualization, Writing—review & editing. P.F.: Conceptualization, Methodology, Writing—review & editing, Supervision

Funding Open access funding provided by Università degli Studi G. D'Annunzio Chieti Pescara within the CRUI-CARE Agreement.

Declarations

Conflict of interest The authors declare that they have no conflict of interest.

Appendix 1: Basic concepts of limit analysis theory

The Limit Analysis furnishes an estimate of the load at which a structure collapses relying only on the structural configuration (i.e. geometry, loads, constraints) on the one hand and plasticity conditions on the other hand. The Limit Analysis is based on two theorems i.e. the Lower-Bound theorem and the Upper-Bound theorem based on a static approach and a kinematic approach, respectively. The present work is focused on the Lower-Bound theorem or the static approach and for this reason only this latter approach is recalled in the following.

Static approach of limit analysis

A generic reference load p_{ref} acting on a structure can be multiplied by a scalar load multiplier P_D identifying with $F = P_D p_{ref}$ the static load that acts on the structure ($F = P_D p_{ref}$ can be obviously intended as a distribution of loads acting on the structure). The multiplier P_D can be increased form zero up to a limit value labelled as P_u for which the stress distribution in the structure is statically and plastically admissible, i.e the corresponding stress field is in equilibrium with the applied load $F_u = P_u p_{ref}$ and in the whole structure, the yield condition is satisfied as $f(\boldsymbol{\sigma}) \leq 0$. This procedure characterizes the static approach of the Limit Analysis in which the safety scalar load multiplier corresponds to the maximum load multiplier P_D, say P_{LB}, for which the stress distribution in the structure is statically and plastically admissible. For the computed P_{LB} results that $P_{LB} \leq P_u$. Knowing the P_{LB}, a lower bound estimate of the collapse load is given by $F_{LB} = P_{LB} p_{ref}$.

Appendix 2: Flow diagram of the ECM

In Fig. 5 the numerical FE-based procedure of the ECM is reported.

References

1. Kanis JA, Burlet N, Cooper C, Delmas PD, Reginster J-Y, Borgstrom F, Rizzoli R (2008) European guidance for the diagnosis and management of osteoporosis in postmenopausal women. Osteoporos Int 19:399–428. https://doi.org/10.1007/s00198-008-0560-z
2. Akkawi I, Zmerly H (2018) Osteoporosis: current concepts. Joints 14:122–127. https://doi.org/10.1055/s-0038-1660790
3. Unnanuntana A, Gladnick BP, Donnelly E, Lane JM (2010) The assessment of fracture risk. J Bone Jt Surg Am 92:743–753. https://doi.org/10.2106/JBJS.I.00919
4. Faulkner KG (2005) The tale of the T-score: review and perspective. Osteoporos Int 16:347–352. https://doi.org/10.1007/s00198-004-1779-y
5. Wainwright SA, Marshall LM, Ensrud KE, Cauley JA, Black DM, Hillier TA, Hochberg MC, Vogt MT, Orwoll ES (2005) Hip fracture in women without osteoporosis. J Clin Endocrinol Metab 90:2787–2793. https://doi.org/10.1210/jc.2004-1568
6. Bouxsein ML (2005) Determinants of skeletal fragility. Best Pract Res Clin Rheumatol 19:897–911. https://doi.org/10.1016/j.berh.2005.07.004
7. Keaveny TM, Clarke BL, Cosman F, Orwoll ES, Siris ES, Khosla S, Bouxsein ML (2020) Biomechanical Computed Tomography analysis (BCT) for clinical assessment of osteoporosis. Osteoporos Int 31:1025–1048. https://doi.org/10.1007/s00198-020-05384-2
8. Falcinelli C, Whyne C (2020) Image-based finite-element modeling of the human femur. Comput Methods Biomech Biomed Eng 23:1138–1161. https://doi.org/10.1080/10255842.2020.1789863
9. Gustafsson A, Tognini M, Bengtsson F, Gasser TC, Isaksson H, Grassi L (2021) Subject-specific FE models of the human femur predict fracture path and bone

strength under single-leg-stance loading. J Mech Behav Biomed Mater 113:104118. https://doi.org/10.1016/j.jmbbm.2020.104118
10. Gaziano P, Falcinelli C, Vairo G (2022) A computational insight on damage-based constitutive modelling in femur mechanics. Eur J Mech A Solids 93:104538. https://doi.org/10.1016/j.euromechsol.2022.104538
11. Lee Y, Ogihara N, Lee T (2019) Assessment of finite element models for prediction of osteoporotic fracture. J Mech Behav Biomed Mater 97:312–320. https://doi.org/10.1016/j.jmbbm.2019.05.018
12. Cody DD, Gross GJ, Hou FJ (1999) Femoral strength is better predicted by finite element models than QCT and DXA. J Biomech 32:1013–1020. https://doi.org/10.1016/s0021-9290(99)00099-8
13. Dragomir-Daescu D, Op Den Buijs J, McEligot S, Dai Y, Entwistle RC, Salas C, Melton LJ, Bennet KE, Khosla S, Amin S (2011) Robust QCT/FEA models of proximal femur stiffness and fracture load during a sideways fall on the hip. Ann Biomed 39:742–755. https://doi.org/10.1007/s10439-010-0196-y
14. Johannesdottir F, Thrall E, Muller J, Keaveny TM, Kopperdahl DL, Bouxsein ML (2017) Comparison of non-invasive assessments of strength of the proximal femur. Bone 105:93–102. https://doi.org/10.1016/j.bone.2017.07.023
15. Falcinelli C, Schileo E, Balistreri L, Baruffaldi F, Bordini B, Viceconti M, Albisinni U, Ceccarelli F, Milandri L, Toni A, Taddei F (2014) Multiple loading conditions analysis can improve the association between finite element bone strength estimates and proximal femur fractures: a preliminary study in elderly women. Bone 67:71–80. https://doi.org/10.1016/j.bone.2014.06.038
16. Qasim M, Farinella G, Zhang J, Li X, Yang L, Eastell R, Viceconti M (2016) Patient-specific finite element estimated femur strength as a predictor of the risk of hip fracture: the effect of methodological determinants. Osteoporos Int 27:2815–2822. https://doi.org/10.1007/s00198-016-3597-4
17. Bhattacharya P, Altai Z, Qasim M, Viceconti M (2019) A multiscale model to predict current absolute risk of femoral fracture in a postmenopausal population. Biomech Model Mechanobiol 18:301–319. https://doi.org/10.1007/s10237-018-1081-0
18. Fleps I, Pàlsson H, Baker A, Enns-Bray W, Bahaloo H, Danner M, Singh NB, Taylor WR, Sigurdsson S, Gudnason V, Ferguson SJ, Helgason B (2022) Finite element derived femoral strength is a better predictor of hip fracture risk than aBMD in the AGES Reykjavik study cohort. Bone 154:1162199. https://doi.org/10.1016/j.bone.2021.116219
19. Ng TP, Koloor SSR, Djuansjah JRP, Abdul Kadir MR (2017) Assessment of compressive failure process of cortical bone materials using damage-based model. J Mech Behav Biomed Mater 66:1–11. https://doi.org/10.1016/j.jmbbm.2016.10.014
20. Marco M, Giner E, Caeiro-Rey JR, Miguelez MH, Larrainzar-Garijo R (2019) Numerical modelling of hip fracture patterns in human femur. Comput Methods Programs Biomed 173:67–75. https://doi.org/10.1016/j.cmpb.2019.03.010
21. Bouxsein ML, Zysset P, Gluer CC, McClung M, Biver E, Pierroz DD, Ferrari SL (2020) Perspectives on the non-invasive evaluation of femoral strength in the assessment of hip fracture risk. Osteoporos Int 31:393–408. https://doi.org/10.1007/s00198-019-05195-0
22. Mirzaei M, Alavi F, Allaveisi F, Naeini V, Amiri P (2018) Linear and nonlinear analyses of femoral fractures: computational/experimental study. J Biomech 79:155–163. https://doi.org/10.1016/j.jbiomech.2018.08.003
23. Pisano AA, Fuschi P, De Domenico D (2012) A layered limit analysis of pinned-joint composite laminates: numerical versus experimental findings. Compos B Eng 43:940–952. https://doi.org/10.1016/j.compositesb.2011.11.030
24. Pisano AA, Fuschi P, De Domenico D (2015) Numerical limit analysis of steel-reinforced concrete walls and slabs. Comput Struct 160:42–55. https://doi.org/10.1016/j.compstruc.2015.08.004
25. Pisano AA, Fuschi P (2021) Limit analysis of human proximal femur. J Mech Behav Biomed Mater 124:104844. https://doi.org/10.1016/j.jmbbm.2021.104844
26. Pisano AA, Fuschi P (2023) Peak load prediction of human bone proximal femur: sensitivity to tissues strength and geometry. In: Garcea G, Weichert D (eds) Direct methods for limit state of materials and structures-advanced computational algorithms and material modelling. Lecture notes in applied and computational mechanics, vol 101. Springer, New York, pp 87–106. https://doi.org/10.1007/978-3-031-29122-7_5
27. Zohar Y, Plitman Mayo R, Dahan G, Trabelsi N, Amir G, Milgrom C (2014) Predicting the stiffness and strength of human femurs with real metastatic tumors. Bone 69:180–190. https://doi.org/10.1016/j.bone.2014.09.022
28. Schileo E, Dall'Ara E, Taddei F, Malandrino A, Schotkamp T, Baleani M, Viceconti M (2008) An accurate estimation of bone density improves the accuracy of subject-specific finite element models. J Biomech 41:2483–2491. https://doi.org/10.1016/j.jbiomech.2008.05.017
29. San Antonio T, Ciaccia M, Muller-Karger C, Casanova E (2012) Orientation of orthotropic material properties in a femur FE model: a method based on the principal stresses directions. Med Eng Phys 34:914–919. https://doi.org/10.1016/j.medengphy.2011.10.008
30. Tellache M, Pithioux M, Chabrand P, Hochard C (2009) Femoral neck fracture prediction by anisotropic yield criteria. Eur J Comput Mech 18:33–41. https://doi.org/10.3166/ejcm.18.33-41
31. Pithioux M, Lasaygues P, Chabrand P (2002) An alternative ultrasonic method for measuring the elastic properties of cortical bone. J Biomech 35:961–968. https://doi.org/10.1016/S0021-9290(02)00027-1

32. Keyak JH, Kaneko TS, Tehranzadeh J, Skinner HB (2005) Predicting proximal femoral strength using structural engineering models. Clin Orthop Relat Res 437:219–228. https://doi.org/10.1097/01.blo.0000164400.37905.22
33. Tsai SW, Wu EM (1971) A general theory of strength for anisotropic materials. J Compos Mater 5:58–80. https://doi.org/10.1177/002199837100500106
34. Pisano AA, Fuschi P (2007) A numerical approach for limit analysis of orthotropic composite laminates. Int J Numer Methods Eng 70:71–93. https://doi.org/10.1002/nme.1872
35. Pisano AA, Fuschi P, De Domenico D (2013) Peak load prediction of multi-pin joints FRP laminates by limit analysis. Compos Struct 96:763–772. https://doi.org/10.1016/j.compstruct.2012.09.038
36. De Domenico D, Pisano AA, Fuschi P (2014) A FE-based limit analysis approach for concrete elements reinforced with FRP bars. Compos Struct 107:594–603. https://doi.org/10.1016/j.compstruct.2013.08.039
37. Pisano AA, Fuschi P, De Domenico D (2013) Peak loads and failure modes of steel-reinforced concrete beams: predictions by limit analysis. Eng Struct 56:477–488. https://doi.org/10.1016/j.engstruct.2013.05.030